Fluid Phase Equilibria 423 (2016) 190–202

Contents lists available at ScienceDirect

Fluid Phase Equilibria

journal homepage: www.elsevier.com/locate/fluid

The effect of *n* vs. *iso* isomerization on the thermophysical properties of aromatic and non-aromatic ionic liquids

Ana S.M.C. Rodrigues [a, **], Hugo F.D. Almeida [b], Mara G. Freire [b], Jose A. Lopes-da-Silva [c], João A.P. Coutinho [b], Luís M.N.B.F. Santos [a, *]

[a] CIQUP, Departamento de Química e Bioquímica, Faculdade de Ciências da Universidade do Porto, R. Campo Alegre 687, P-4169-007 Porto, Portugal
[b] CICECO, Departamento de Química, Universidade de Aveiro, P-3810-193 Aveiro, Portugal
[c] QOPNA, Departamento de Química, Universidade de Aveiro, P-3810-193 Aveiro, Portugal

ARTICLE INFO

Article history:
Received 24 February 2016
Received in revised form
8 April 2016
Accepted 10 April 2016
Available online 13 April 2016

Keywords:
Ionic liquids
Density
Viscosity
Heat capacity
Refractive index
Surface tension
Glass transition
Phase behaviour
Imidazolium
Pyridinium
Piperidinium
Pyrrolidinium
Bis(trifluoromethylsulfonyl)imide
Differential scanning calorimetry
Isomerization

ABSTRACT

This work explores the *n* vs. *iso* isomerization effects on the physicochemical properties of different families of ionic liquids (ILs) with variable aromaticity and ring size. This study comprises the experimental measurements, in a wide temperature range, of the ILs' thermal behaviour, heat capacities, densities, refractive indices, surface tensions, and viscosities. The results here reported show that the presence of the *iso*-alkyl group leads to an increase of the temperature of the glass transition, T_g. The *iso*-pyrrolidinium (5 atoms ring cation core) and *iso*-piperidinium (6 atoms ring cation core) ILs present a strong differentiation in the enthalpy and entropy of melting. Non-aromatic ILs have higher molar heat capacities due to the increase of the atomic contribution, whereas it was not found any significant differentiation between the *n* and *iso*-alkyl isomers. A small increase of the surface tension was observed for the non-aromatic ILs, which could be related to their higher cohesive energy of the bulk, while the lower surface entropy observed for the *iso* isomers indicates a structural resemblance between the IL bulk and surface. The significant differentiation between ILs with a 5 and 6 atoms ring cation in the *n*-alkyl series (where 5 atoms ring cations have higher surface entropy) is an indication of a more efficient arrangement of the non-polar region at the surface in ILs with smaller cation cores. The ILs constituted by non-aromatic piperidinium cation, and *iso*-alkyl isomers were found to be the most viscous among the studied ILs due to their higher energy barriers for shear stress.

1. Introduction

Most of the research on the structural property relationships of ionic liquids (ILs) is focus on the effect that major structural variations, such as alkyl side chain length, and the nature of anions and cations, have on their thermophysical properties [1–8]. The complexity and variety of ILs make the rationalization of these relationships hard, yet amenable, and a large number of approaches to predict the properties of ionic liquids has been proposed [8–16]. However, few studies highlight small structural variations on ILs, such as isomerization, or chemical nature differentiation (e.g. aromatic vs. aliphatic and ammonium vs. phosphonium) and their effect on the ILs thermophysical properties [17–30]. However, the understanding and development of structure-property relationships are important from both fundamental and applied standpoints. It allows a rationalization of the molecular level interactions and the development of heuristics and correlations that allow the design of ionic liquids for specific applications.

Previous studies suggested that the branching of the alkyl side chain not affect their density significantly, but when some cycle group (aromatic and non-aromatic) is present in the alkyl chain, the densities increase [20,23,26]. Regarding transport properties, such as viscosity, a small variation of the aliphatic side group may lead to substantial changes in their properties [23,25];as the nanostructuration of ILs becomes highly affected a significant impact

* Corresponding author.
** Corresponding author.
E-mail addresses: asmcrodrigues@fc.up.pt (A.S.M.C. Rodrigues), lbsantos@fc.up.pt (L.M.N.B.F. Santos).

http://dx.doi.org/10.1016/j.fluid.2016.04.009
0378-3812/

occurs in the shear stress of ILs. Aromatic ILs with branched and cyclic alkyl side chains were shown to have higher viscosities than their *n*-alkyl homologous [20,23]. For different cyclic groups in the alkyl chain or the cation core, the viscosity is expected to be dependent on the size and structure of the cyclic group and in the magnitude of dispersive intermolecular interactions (van der Waals). The relatively high viscosity for these ILs compared with their *n*-alkyl homologous depends heavily on the reorientation motion on ILs. Maginn and co-workers [28], based on the unpublished data by Xue et al. [31], reported higher viscosities for branched aromatic ILs. According to the simulation study carried by the authors [28] these results were explained by a higher packing stability of the ion pairs in the liquid phase. In summary, the viscosity is highly affected by the specific shape and length of the ILs alkyl side chain.

There are few works concerning the thermal behaviour of isomeric ILs. Quitevis et al. [26] have shown that changing from aromatic to non-aromatic alkyl substituents has a significant effect on the thermal properties of ILs. Generally, ILs with aromatic and branched substituted cations show higher T_g values than their aliphatic analogs, regardless of the anion [29].

In this work, we investigated the structure–property relationships regarding the effect of *n*-butyl versus *iso*-butyl substituents in aromatic (imidazolium and pyridinium) and non-aromatic (pyrrolidinium and piperidinium) cations of $[NTf_2]^-$-based ILs. These ILs were chosen in order to study the effect of a branched alkyl side chain on aromatic and aliphatic cations on several thermophysical properties, such as thermal behaviour, heat capacities, densities, refractive indices, surface tensions, and viscosities.

2. Experimental section

2.1. Materials and purification

All ILs were purchased from IoLiTec with the highest purity available. The ILs samples were maintained dried under vacuum ($p < 0.1$ Pa) at moderate temperature (323 K) and constant stirring up to the measurements, to remove traces of the most volatile impurities and moisture. The purity of each IL was checked by NMR spectroscopy (^{1}H and ^{13}C). For detailed NMR analysis, see Supporting Information. The water mass fraction contents were determined with a Metrohm 831 Karl Fischer coulometer, using the Hydranal-Coulomat AG® from Riedel-de Haën. Table 1 presents the list of the studied ILs, their abbreviation, molar masses, purity, and the water content while Fig. 1 provides a schematic representation of the ILs studied. The relative atomic masses used in this work were those recommended by the IUPAC Commission in 2007 [32].

2.2. Thermal behaviour

Glass transition (temperatures and molar heat capacity change), enthalpies and entropies of melting of the ILs under study were measured in a power compensation differential scanning calorimeter, PERKIN ELMER model Pyris Diamond DSC, previously calibrated with some reference materials [33,34]. The methodology adopted in the phase behaviour study is provided in the Supporting Information. The calibration and the ILs phase behaviour study were performed using the same experimental methodology to improve the resolution of the differential analysis of this study. The $[C_6C_1im][NTf_2]$ ionic liquid was used as a reference test sample for the DSC calibration and methodology adopted in this work. The experimental results for the $[C_6C_1im][NTf_2]$ were compared with the literature values determined by Paulechka et al. [35]· [36] measured with adiabatic calorimetry.

2.3. Heat capacities

The ILs heat capacities at $T = 298.15$ K were measured by a high-precision heat capacity drop calorimeter described in the literature [37–39]. The calorimeter was calibrated with water and sapphire (α-Al_2O_3) [33]. The calibration constant was found to be $\varepsilon = (6.6040 \pm 0.0036)\ W \cdot V^{-1}$. The ampoules were weighted in a Mettler Toledo AG245 dual range analytical balance (sensitivity of 1×10^{-5} g and repeatability of 2×10^{-5} g) both empty and after filling with the ionic liquid. The accuracy and resolution of the apparatus for measurements of heat capacities of liquids and solids were previously evaluated using hexafluorobenzene, *p*-terphenyl, benzoic acid, and $[C_6C_1im][NTf_2]$ [39]. All uncertainties are given as twice of the standard deviation of the average value and include the calibration uncertainty. The buoyancy effect correction was considered for both the calibration and ILs measurements.

2.4. Densities and viscosities

The density, ρ, and viscosity, η, of the pure ILs were measured using an automated SVM 3000 Anton Paar rotational Stabinger viscometer – densimeter. The apparatus was calibrated in the same experimental conditions of the ionic liquid measurements, using three standard calibration samples: APN7.5 (9.995 $mPa \cdot s^{-1}$/0.8159 g. cm^{-3}), APN26 (50.02 $mPa \cdot s^{-1}$/0.8209 $g \cdot cm^{-3}$), and APN415 (1105 $mPa \cdot s^{-1}$0.8456 $g \cdot cm^{-3}$) (values at 293.15 K). The reproducibility of the dynamic viscosity and density measurements is, according to the manufacturer, 0.35% and ± 0.5 $kg \cdot m^{-3}$, respectively, from 288.15 to 378.15 K, and the uncertainty of temperature is within ± 0.02 K. The measurements were carried out at

Table 1
IUPAC names, abbreviation, molar masses (*MM*) and water content for each studied ionic liquid.

Ionic liquid	Abbreviation	*MM*/g mol^{-1}	Water content (ppm)	Purity[a]
1-(2-methylpropyl)-3-methylimidazolium bis(trifluoromethylsulfonyl)imide	$[iC_4C_1im][NTf_2]$	419.366	20	>98% (NMR); <100 ppm Halides (IC)
1-butyl-3-methylpyridinium bis(trifluoromethylsulfonyl)imide	$[C_4C_1py][NTf_2]$	430.389	62	99% (NMR) <100 ppm Halides (IC)
1-(2-methylpropyl)-3-methylpyridinium bis(trifluoromethylsulfonyl)imide	$[iC_4C_1py][NTf_2]$	430.389	28	98% (NMR) <100 ppm Halides (IC)
1-butyl-1-methylpyrrolidinium bis(trifluoromethylsulfonyl)imide	$[C_4C_1pyrr][NTf_2]$	422.410	55	99% (NMR) <100 ppm Halides (IC)
1-(2-methylpropyl)-1-methylpyrrolidinium bis(trifluoromethylsulfonyl)imide	$[iC_4C_1pyrr][NTf_2]$	422.410	21	98% (NMR) <100 ppm Halides (IC)
1-butyl-1-methylpiperidinium bis(trifluoromethylsulfonyl)imide	$[C_4C_1pip][NTf_2]$	436.437	70	99% (NMR) <100 ppm Halides (IC)
1-(2-methylpropyl)-1-methylpiperidinium bis(trifluoromethylsulfonyl)imide	$[iC_4C_1pip][NTf_2]$	436.437	17	98% (NMR) <100 ppm Halides (IC)

[a] Purity from the supplier: ^{1}H NMR (Nuclear magnetic resonance), Ionic chromatography (IC).

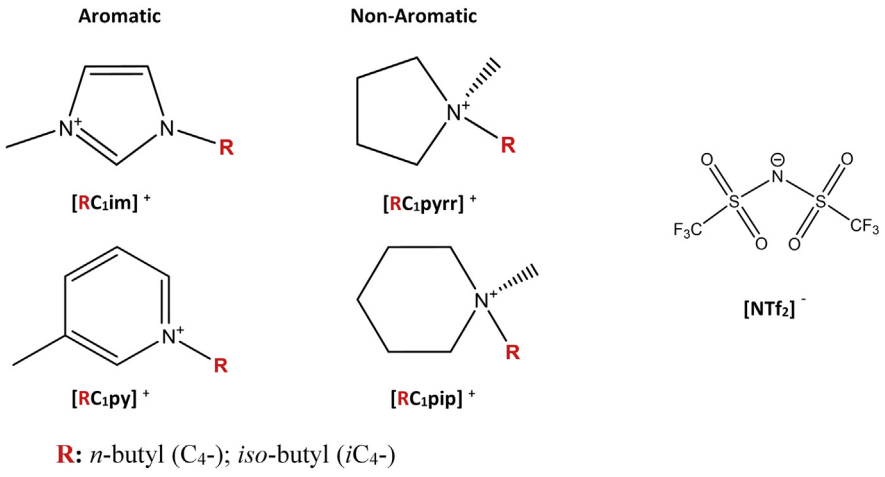

Fig. 1. Schematic representation of the ILs under study. Aromatic ILs: [iC_4C_1im][NTf_2]; [C_4C_1py][NTf_2]; [iC_4C_1py][NTf_2]; Non-aromatic ILs: [C_4C_1pip][NTf_2]; [iC_4C_1pip][NTf_2]; [C_4C_1pyrr][NTf_2]; [iC_4C_1pyrr][NTf_2].

pressure, $p^\circ = 0.10 \pm 0.01$ MPa, in the temperature range from (278.15–363.15) K. The [iC_4C_1pip][NTf_2] ionic liquid (solid at room temperature), was determined in the temperature range from 303.15 to 363.15 K. For each ionic liquid, at least, two independent measurements were performed, using the same experimental conditions and different samples.

2.5. Surface tension

The surface tension of each ionic liquid sample was determined by the analysis of the shape of a pendant drop and measured using a Dataphysics (model OCA-20) contact angle system. The temperature inside the aluminium chamber in which the surface tensions were determined was measured with a Pt100 within ±0.1 K (placed at a distance of approximately 20 mm from the liquid drop). After reaching a specific temperature inside the aluminium chamber, the measurements were carried out 40 min after, to guarantee thermal stabilization. Silica gel was kept inside the air chamber to maintain a dry environment. Drop volumes of 9 ± 0.5 μL were obtained using a Hamilton DS 500/GT syringe connected to a Teflon coated needle placed inside an aluminium air chamber able to maintain the temperature of interest within ± 0.1 K. The analysis of the drop shape was done with the software module SCA 20, where the gravitational acceleration ($g = 9.801(8)$ m·s^{-2}) and latitude (lat. = 40°, sea level) were used, according to the location of the assay. The surface tensions were calculated using the measured density data. For the surface tensions determination at each temperature, and for each ionic liquid, at least, 5 drops were formed and analysed. For each drop, an average of 150 images was captured. The surface tension measurements were performed in the temperature range from 298.15 to 343.15 K, except the [iC_4C_1pip][NTf_2], which is solid at room temperature, and the measurements were performed in the temperature range from 308.4 to 343.0 K. In order to validate the equipment and methodology used, the surface tension of ultra-pure and deionised water, *n*-decane, and *n*-dodecane were determined from (298–343) K, and are in close agreement with literature values [40–42]. Also the surface tensions of [C_4mim][PF_6], [C_4mim][Ntf_2], [C_4mim][CF_3SO_3], and [C_4mim][BF_4] were determined in the temperature interval between (298 and 343) K, using the density values for the [C_4mim]-based ionic liquids taken from literature [43–45], and were compared with previous results published by us using the du Noüy ring method [46,47]. Further details on the equipment and its validity to measure surface tensions of ILs can be found in supporting information.

2.6. Refractive indices

The refractive indices of ILs were measured at the sodium D-line using a Bellingham model RFM 340 refractometer ($\pm 3 \times 10^{-5}$ stated precision), as a function of temperature. The refractometer features a presser with a seal ring made of fluoropolymer Kalrez® which is closed over the sample on the sapphire prism. The presser incorporates a micro flow cell, which is used to introduce the sample into the refractometer, without opening the presser. The presser and the internal prism water jacket assembly is temperature controlled by an external bath through the presser hinge and integral channels in the presser arm. The temperature in the refractometer cell is controlled using an external thermostatic bath within a temperature fluctuation of $\pm 5 \times 10^{-3}$ K, measured with a resolution better than 1×10^{-3} K and an uncertainty within ±0.02 K. The apparatus was calibrated with degassed water (Millipore quality) and toluene (Spectranal, 99.9%). Samples were directly introduced into the flow cell (prism assembly) using a syringe; the flow cell was kept closed after sample injection. For each ionic liquid, at least, two independent experiments were performed and in each experiment, at least, three measurements were taken at each temperature. The refractive indices were measured with respect to air and no corrections were applied.

3. Results and discussion

3.1. Thermal behaviour

The experimental results concerning the thermal behaviour of the ILs investigated are summarized in Table 2. Fig. 2 depicts the glass temperatures of the *n* and *iso*-butyl isomers. [iC_4C_1pyrr][NTf_2] could not form a glass, since it crystallizes in the cooling quenching process performed in this work. The thermograms and some experimental details are presented as Supporting Information. The nomenclature used in this paper section relatively to the phase transitions is follow described: s: solid; gs: glass-state; sl: supercooled-liquid; l: liquid. The enthalpies and entropies of melting were corrected to the reference temperature of $T = 298.15$ K, according to equations (1) and (2), respectively:

Table 2
Glass transition, T_g, solid-solid, T_{ss}, and melting, T_m, temperatures. Heat capacity change of the glass transition, $\Delta^{sl}_{gs}C^{\circ}_{p,m}$, and enthalpy, $\Delta_{trs}H^{\circ}_{m}$, and entropy, $\Delta_{trs}S^{\circ}_{m}$ of phase transitions for the studied ILs at $p^{\circ} = 0.10 \pm 0.01$ MPa.

Ionic liquid anion $[NTf_2]^-$	T/K	$\Delta^{sl}_{gs}C^{\circ}_{p,m}$/J K^{-1} mol^{-1}	$\Delta_{trs}H^{\circ}_{m}$/kJ mol^{-1}	$\Delta_{trs}S^{\circ}_{m}$/J K^{-1} mol^{-1}
Cations				
$[C_6C_1im]^+$	184.4 (T_g)	171		
	[184.3[b]; 192[c]; 189[d]] (T_g)			
	262.6 (T_m)			
	[267[c]; 272.03[e]] (T_m)			
$[C_4C_1im]^+$	181.3 (T_g)[b]	74[e]		
$[iC_4C_1im]^+$	190.6 (T_g)	94		
$[C_4C_1py]^+$	185.2 (T_g)	70		
$[iC_4C_1py]^+$	193.6 (T_g)	101		
$[C_4C_1pyrr]^+$	183.0 (T_g)	83		
	259.7(T_m)		20.2 ± 0.7 (T_m)	77.8 ± 2.7 (T_m)
	[265.65 ± 0.05[f]] (T_m)		[21.9 ± 0.1][f]	
	(0.70) [g]		24.1 ± 0.7 (298.15 K)	91.7 ± 2.7 (298.15 K)
$[iC_4C_1pyrr]^+$	253.0 (T_{ss})		4.1 ± 0.7 (T_{ss})	16.2 ± 2.7 (T_{ss})
	272.9 (T_m)		13.1 ± 0.7 (T_m)	48.0 ± 2.6 (T_m)
			19.7 ± 1.0 (298.15 K)	73.1 ± 3.7 (298.15 K)
$[C_4C_1pip]^+$	194.8 (T_g)	73		
$[iC_4C_1pip]^+$	194.8 (T_g)	[i]	1.0 ± 0.7 (T_{ss})	4.2 ± 2.9 (T_{ss})
	239.5 (T_{ss})		19.3 ± 0.7 (T_{trans})[h]	70.7 ± 2.6 (T_{trans})[h]
	273.1 (T_{trans})[h]		2.4 ± 0.7 (T_m)	8.3 ± 2.4 (T_m)
	287.9 (T_m)		23.7 ± 1.2 (298.15 K)	86.7 ± 4.6 (298.15 K)
	(0.71)[g]			

The expanded uncetainty, within 0.95 confidence level, of the experimental results, was taken as the extended standard deviation for the enthalpies of melting, σ, and was estimated as ± 0.5 K for the T_g and T_m. $\Delta_{trs}H^{\circ}_{m}$ stands for the enthalpy of various transitions identified as: solid-solid, T_{ss}, and melting, T_m. The enthalpies and entropies were corrected at 298.15 K using $\Delta^{l}_{s}C^{\circ}_{p,m} = 101\ J\cdot K^{-1}\cdot mol^{-1}$ and $\Delta^{s}_{s}C^{\circ}_{p,m} = 0\ J\cdot K^{-1}\cdot mol^{-1}$ and corresponds to the sum of all the enthalpy changes from the most stable crystal form to the isotropic liquid. An uncertainty of $10\ J\cdot K^{-1}\cdot mol^{-1}$ was estimated for $\Delta^{sl}_{gs}C^{\circ}_{p,m}$. Literature data: [b] [50];[c] [48];[d] [49] (differential scanning calorimetry), [e] [36]; [f] [51] (adiabatic calorimetry); [g] ratio between T_g/T_m. [h] The ration between the enthalpy of melting (isotropization) and this transition is in order of 13%, which indicate that this transition could correspond to a solid to crystal liquid phase transition. [i] The $\Delta^{sl}_{gs}C^{\circ}_{p,m}$ could not be determined because a partial crystallization occurred (see supporting information).

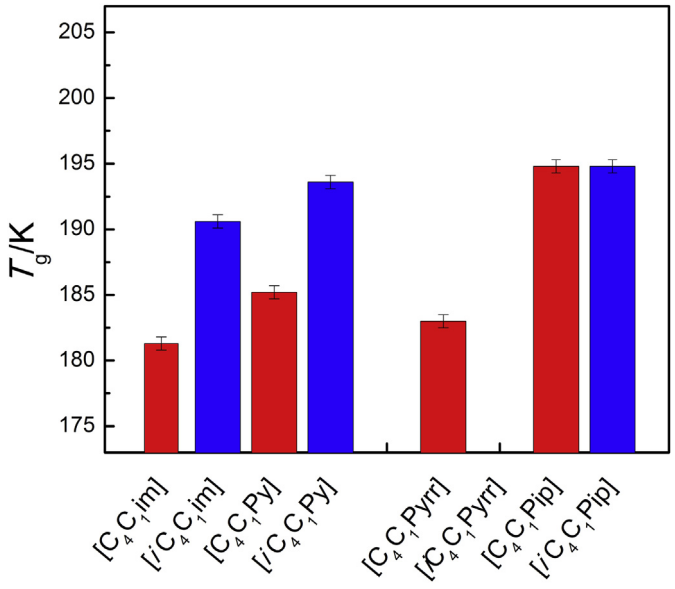

Fig. 2. Glass transition temperatures as a function of the *n* and *iso*-butyl cations of $[NTf_2]^-$ – based ILs.

$$\Delta^{l}_{s}H^{\circ}_{m}(298.15K) = \Delta^{l}_{s}H^{\circ}_{m}\left(T_{fus}\right) + \Delta^{l}_{s}C^{\circ}_{p,m}\left(298.15 - T_{fus}\right) \quad (1)$$

$$\Delta^{l}_{s}S^{\circ}_{m}(298.15K) = \Delta^{l}_{s}H^{\circ}_{m}\left(T_{fus}\right)/T_{fus} + \Delta^{l}_{s}C^{\circ}_{p,m}\Delta\ln\left(298.15/T_{fus}\right) \quad (2)$$

The molar heat capacity differences between the liquid and the solid, $\Delta^{l}_{s}C^{\circ}_{p,m}$, used in the corrections of the enthalpies and entropies of melting, at $T = 298.15$ K, were estimated based on the respective molar heat capacity change, $\Delta^{l}_{gs}C^{\circ}_{p,m}$, at glass transition (typical ratio between the heat capacities changes, $\Delta^{l}_{gs}C^{\circ}_{p,m}/\Delta^{l}_{s}C^{\circ}_{p,m} = 0.8$), taking into account our results for $[C_6C_1im][NTf_2]$ and the data reported by Paulechka et al. for the same IL [35,36]. The experimental data of the enthalpies of transition, at the transition temperatures, are provided in Table 2. The molar heat capacity change associated with glass transition, $\Delta^{l}_{gs}C^{\circ}_{p,m}$, determined in this work corresponds to the difference between the molar heat capacities of the supercooled liquid $C^{\circ}_{p,m}(l)$ and glass state $C^{\circ}_{p,m}(gs)$, according to equation (3).

$$\Delta^{l}_{gs}C^{\circ}_{p,m} = C^{\circ}_{p,m}(l) - C^{\circ}_{p,m}(gs) \quad (3)$$

The glass and melting transition temperatures obtained for $[C_6C_1im][NTf_2]$, presented in Table 2, are in agreement with literature results [35,36,48,49]. The reported overall uncertainties are twice the standard deviation of the average value. The uncertainties of the experimental results were assigned on the basis of the extended standard deviation of the experimental and the calibration results. The entropy, at $T = 298.15$ K, of the transition was determined by equation (4):

$$\Delta^{l}_{s}S^{\circ}_{m}(298.15\ K) = \Delta^{l}_{s}H^{\circ}_{m}(298.15\ K)/298.15 \quad (4)$$

The results presented in Fig. 2 show a strong differentiation in the glass temperatures between *n* and *iso*-alkyl ILs. The *iso*-alkyl aromatic ILs (imidazolium- and pyridinium-based) have higher glass temperatures than their respective *n*-alkyl isomers, meaning a high relative glass stability, as discussed by Maginn and co-workers [28] for imidazolium-based ILs. The glass state resembles the freezing state of the isotropic liquid. Its relative stability is driven mostly by the size and the magnitude of the interactions in the bulk IL. The higher T_g for the piperidinium-based ILs indicates higher conformational entropy relative to the pyrrolidinium and the

remaining ILs formed by different cations (aromatic and non-aromatic). These results are consistent with the fact that piperidinium is a more flexible cation with a larger number of possible conformers. Additionally, these results can be associated with an additional increase of the absolute entropy of both glass and the liquid phases, leading to a lower heat capacity change ($73\ J\cdot K^{-1}\cdot mol^{-1}$) at the glass transition (which is an evidence of a smaller entropic differentiation between the glass and the supercooled liquid) and, as a consequence, to an increase of the glass temperature. Unlike observed for the aromatic ILs, no significant effect of the *iso*-alkyl on the glass transition was observed for non-aromatic ILs, mainly because the contribution of the dispersive interactions of the cation surpasses in magnitude any effect that the *iso*-alkyl may have in glass transition.

The melting temperature of the *iso*-alkyl pyrrolidinium IL is higher than the *n*-alkyl isomer by about 13 K, as reported in Table 2. This difference has an enthalpic contribution of $3\ kJ\cdot mol^{-1}$ but it is essentially entropically driven, indicating a lower conformation entropy of $[iC_4C_1pyrr][NTf_2]$ in the liquid bulk. The observed difference of 15 K in the melting temperature between the *iso*-pyrrolidinium (5 atoms ring cation core) and *iso*-piperidinium (6 atoms ring cation core) is strongly enthalpically driven.

3.2. Heat capacities

The molar, $C^{o}_{p,m}(J\cdot K^{-1}\cdot mol^{-1})$, specific, c^{o}_{p} $(J\cdot K^{-1}\cdot g^{-1})$, and volumic, $C^{o}_{p}/V(J\cdot K^{-1}\cdot cm^{-3})$ heat capacities, at $T = 298.15$ and $p^{\circ} = 0.10 \pm 0.01$ MPa, are presented in Table 3. The molar heat capacities of the non-aromatic ILs are, as expected, higher than the aromatic ILs due to the increase of the atomic contribution. There is no significant difference between the *n* and *iso* isomers, in agreement with the observed in other compounds (e.g. the molar heat capacity of butane, $130.2\ J\cdot K^{-1}\cdot mol^{-1}$ at $T = 260$ K [52], and *iso*-butane, $129.7\ J\ K^{-1}\ mol^{-1}$ at $T = 260$ K [53]). A consistent difference is, however, observed between the heat capacity of the analogous aromatic and the non-aromatic molecules, in the order of $20\ J\ K^{-1}\ mol^{-1}$, in agreement with the expected heat capacity increment contribution (at 298.15 K) of five additional atoms in the cation core. The volumic heat capacity, at $T = 298.15$ K, determined in this work, $(1.90–1.94)\ J\cdot K^{-1}\cdot cm^{-3}$, is in the range of the typical average value of $1.92\ J\cdot K^{-1}\cdot cm^{-3}$, which was previously suggested in the literature and verified after for the homologous series $[C_nC_1im][NTf_2]$ with an alkyl chain length above Critical Alkyl Size (CAS), at $n = 6$. The critical alkyl size, starting from $n = 6$ of the *n* alkanes in the $[C_nC_1im][NTf_2]$ corresponds to the point where the Ils starts to evidence the nanostructuration [51,54,55].

3.3. Densities

The experimental density data for the ILs as a function of temperature is presented in Table 4. The density data (ρ) was further correlated with temperature (T) using a second order polynomial equation (5):

$$\ln\left(\rho/g\cdot cm^{-3}\right) = a + b\cdot T + c\cdot T^2 \tag{5}$$

where a, b, and c are the coefficients obtained by the least square fitting method. The graphic representation of the logarithm of the density as a function of temperature is shown in Fig. 3.

The isobaric thermal expansion coefficient, α_p, which considers the volumetric changes with temperature, was using equation (6), derived from equation (5):

$$\alpha_p = -\frac{1}{\rho}\left(\frac{\partial\rho}{\partial T}\right)_p = -\left(\frac{\partial \ln \rho}{\partial T}\right)_p = -[b + 2c\cdot(T/K)] \tag{6}$$

where, ρ is the density in kg m^{-3}, T is the temperature in K, p is the standard pressure ($p^{\circ} = 0.10 \pm 0.01$ MPa), and b and c are the fitted coefficients from the equation (5). The derived a, b, and c coefficients, the molar volume and the thermal expansion coefficients, at $T = 323.15$ K and $p^{\circ} = 0.10 \pm 0.01$ MPa, for all the studied ILs are listed in Table 5. Since the $[iC_4C_1pip]$ is solid at room temperature, the comparison of the data for all the thermophysical properties was done at $T = 323.15$ K. The graphic representations of the density and molar volume and thermal expansion coefficients at 323.15 K and $p^{\circ} = 0.10 \pm 0.01$ MPa, against the different cations are depicted in Fig. 4 (I) and (II) and Fig. 5, respectively.

The comparison of the densities at $T = 323.15$ K, depicted in Fig. 4 (I), reveals a differentiation between aromatic and non-aromatic ILs. Aromatic ILs are denser than the respective non-aromatic ILs due to the planarity of the aromatic moieties and aromatic interactions. There is, however, no significant difference between the *n* and *iso* isomers, in agreement with previous reports. [28], except for the piperidinium cation isomers. Nevertheless, we found that *n* vs. *iso* differentiation in piperidinium Ils (around $10\ kg\cdot m^{-3}$, less than 0.8%) is small and it is very difficult to find a non-speculative and reasonable explanation for that. The thermal expansion is also highly differentiated, within the uncertainty associated, with non-aromatic ILs presenting lower thermal expansion than the aromatic ones; yet, no significant differences are observed between the *n* and *iso* isomers.

3.4. Surface tension

Experimental results of surface tension, γ $(mN\cdot m^{-1})$, at $p^{\circ} = 0.10 \pm 0.01$ MPa for the investigated ILs as a function of temperature are presented in Table 6. The surface thermodynamic properties, namely surface entropy and surface enthalpy, were estimated using the quasi-linear dependence of the surface tension with temperature [57]. The surface entropy, $S^{\gamma}(T)$, was determined according to equation (7), and the surface enthalpy, $H^{\gamma}(T)$, was determined according to equation (8):

Table 3
Molar heat capacity, $C^{o}_{p,m}$ $(J\cdot K^{-1}\cdot mol^{-1})$, specific heat capacity, c^{o}_{p} $(J\cdot K^{-1}\cdot g^{-1})$, and volumic heat capacity, C^{o}_{p}/V $(J\cdot K^{-1}\cdot cm^{-3})$ at 298.15 K and $p^{\circ} = 0.10 \pm 0.01$ MPa.

Ionic liquid anion $[NTf_2]^-$	$C^{o}_{p,m}/J\cdot K^{-1}\cdot mol^{-1}$	$c^{o}_{p}/J\cdot K^{-1}\cdot g^{-1}$	$C^{o}_{p}/V/J\cdot K^{-1}\cdot cm^{-3}$
$[C_4C_1im]^+$ [54]	565.9 ± 0.6	1.349 ± 0.002	1.940 ± 0.002
$[iC_4C_1im]^+$	565.3 ± 0.4	1.348 ± 0.001	1.937 ± 0.002
$[C_4C_1py]^+$	578.1 ± 0.8	1.343 ± 0.002	1.899 ± 0.003
$[iC_4C_1py]^+$	579.0 ± 0.6	1.345 ± 0.002	1.900 ± 0.003
$[C_4C_1pyrr]^+$	584.3 ± 0.6	1.383 ± 0.001	1.939 ± 0.003
$[iC_4C_1pyrr]^+$	582.2 ± 0.6	1.378 ± 0.002	1.930 ± 0.003
$[C_4C_1pip]^+$	607.5 ± 0.8	1.392 ± 0.002	1.924 ± 0.003

The expanded uncertainty, within 0.95 confidence level, of the experimental results, was taken as the extended standard deviation. The expanded uncertainty includes the calibration uncertainty.

Table 4
Experimental results of density, ρ, at $p^\circ = 0.10 \pm 0.01$ MPa for the investigated ILs as a function of temperature.

T/K	ρ/(kg·m^{-3})						
	$[iC_4C_1im]^+$	$[C_4C_1py]$	$[iC_4C_1py]^+$	$[C_4C_1pyrr]^+$	$[iC_4C_1pyrr]^+$	$[C_4C_1pip]^+$	$[iC_4C_1pip]^+$
	$[NTf_2]^-$						
293.15	1442.1	1418.7	1417.2	1406.1	1404.5	1386.9	
298.15	1437.2	1414.1	1412.6	1401.6	1400.0	1382.5	
303.15	1432.4	1409.4	1408.0	1397.2	1395.6	1378.1	1392.9
308.15	1427.7	1404.8	1403.4	1392.7	1391.2	1373.8	1388.6
313.15	1422.9	1400.2	1398.8	1388.3	1386.8	1369.5	1384.4
318.15	1418.2	1395.6	1394.2	1383.8	1382.4	1365.2	1380.1
323.15	1413.5	1391.1	1389.7	1379.4	1378.0	1361.0	1375.9
328.15	1408.8	1386.6	1385.1	1375.1	1373.7	1356.7	1371.7
333.15	1404.2	1382.0	1380.6	1370.7	1369.4	1352.5	1367.5
338.15	1399.5	1377.6	1376.1	1366.4	1365.2	1348.3	1363.3
343.15	1394.9	1373.1	1371.6	1362.1	1360.9	1344.1	1359.1
348.15	1390.3	1368.7	1367.2	1357.8	1356.7	1340.0	1355.0
353.15	1385.7	1364.3	1362.8	1353.6	1352.5	1335.9	1350.8
358.15	1381.1	1359.9	1358.4	1349.3	1348.3	1331.8	1346.7
363.15	1376.6	1355.6	1354.1	1345.1	1344.1	1327.7	1342.7

The expanded uncertainty, within 0.95 confidence level, for the density and temperature data are ± 0.2 kg·m^{-3} and ± 0.02 K respectively. The expanded uncertainty includes the calibration uncertainty.

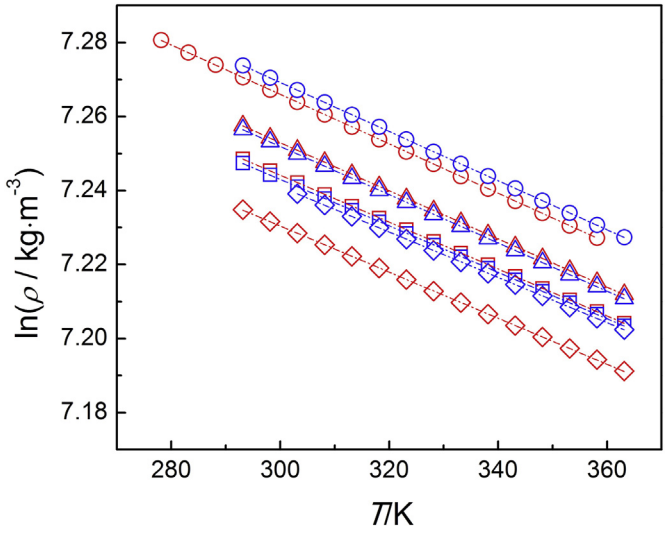

Fig. 3. Logarithm of density as a function of temperature. Literature: (red) ○ -[C_4C_1im][NTf_2] [56]. This work: (blue) ○ - [iC_4C_1im][NTf_2]; (red) △ - [C_4C_1py][NTf_2]; (blue) △ - [iC_4C_1py][NTf_2]; (red) □ - [C_4C_1pyrr][NTf_2]; (blue) □ - [iC_4C_1pyrr][NTf_2]; (red) ◇ - [C_4C_1pip][NTf_2]; (blue) ◇ - [iC_4C_1pip][NTf_2]. (For interpretation of the references to colour in this figure legend, the reader is referred to the web version of this article.)

$$S^\gamma(T) = -\left(\frac{d\gamma}{dT}\right)_T \tag{7}$$

$$H^\gamma(T) = \gamma - T\cdot\left(\frac{d\gamma}{dT}\right)_T \tag{8}$$

where, γ, stands for the surface tension and T for the temperature. The values of the surface tensions and the thermodynamic functions, at $T = 330$ K, of all bis[(trifluoromethyl)sulfonyl]imide-based ILs derived from the temperature dependence of the surface tension, $\gamma = f(T)$, in combination with the associated deviations [58], are presented in Table 7. Fig. 6 (I) depicts the dependence of the surface tension with temperature and the surface tensions, at $T = 330$ K. Surface enthalpies and entropies of the studied ionic liquids are depicted in Fig. 7 (I) and (II), respectively. The surface tension range (~31–33) mN·m^{-1} determined in this work are in the range of the surface tension determined experimentally for the [$C_nC_1$im][NTf_2] series [59]. The surface tensions of ILs are ruled by the preferential orientation of the alkyl group to the surface. Different types of cations (with long alkyl chain) marginally influence the differentiation of the ILs surface tension, since their surface is very similar to alkanes. The slight increase of the surface tension from the aromatic to non-aromatic ring ILs should be related to the expected higher cohesive energy of the bulk in the non-aromatic fluids. The effect of the *iso*-alkyl chain on the surface tension seems to be different for 5 and 6 atom rings. While the former, the *iso* isomers, present a lower surface tension, the effect is negligible, or even opposite, for the latter.

The lower surface entropy of the *iso* isomers is an indication of the high structural resemblance between the bulk and the surface. Again, here a significant differentiation is observed between ILs

Table 5
List of fitted parameters (equation (5)), density, molar volume, and thermal expansion coefficients, α_p, at 323.15 K and $p^\circ = 0.10 \pm 0.01$ MPa for the studied ILs.

Ionic liquid anion $[NTf_2]^-$	a	$10^4 \times b$/K^{-1}	$10^7 \times c$/K^{-2}	ρ/(kg·m^{-3})	V_m/(cm^3·mol^{-1})	$10^3 \times \alpha_p$/K^{-1}
				$T = 323.15$ K		
$[iC_4C_1im]^+$	7.4760 ± 0.0015	−7.11 ± 0.09	0.72 ± 0.14	1409.0	304.5	0.664 ± 0.013
$[C_4C_1py]^+$	7.4633 ± 0.0015	−7.43 ± 0.09	1.41 ± 0.14	1391.1	301.5	0.652 ± 0.013
$[iC_4C_1py]^+$	7.4585 ± 0.0021	−7.19 ± 0.13	1.02 ± 0.20	1390.0	301.8	0.653 ± 0.018
$[C_4C_1pyrr]^+$	7.4471 ± 0.0017	−7.12 ± 0.10	1.19 ± 0.16	1379.4	306.2	0.635 ± 0.022
$[iC_4C_1pyrr]^+$	7.4475 ± 0.0016	−7.26 ± 0.09	1.51 ± 0.14	1378.1	306.5	0.629 ± 0.014
[C4C1pip]$^+$	7.4345 ± 0.0012	−7.28 ± 0.07	1.60 ± 0.11	1361.0	320.7	0.624 ± 0.013
[iC4C1pip]$^+$	7.4306 ± 0.0026	−6.47 ± 0.16	0.52 ± 0.24	1376.0	317.2	0.614 ± 0.012

The uncertainties quoted in the table are the expanded uncertainties with 0.95 level of confidence.

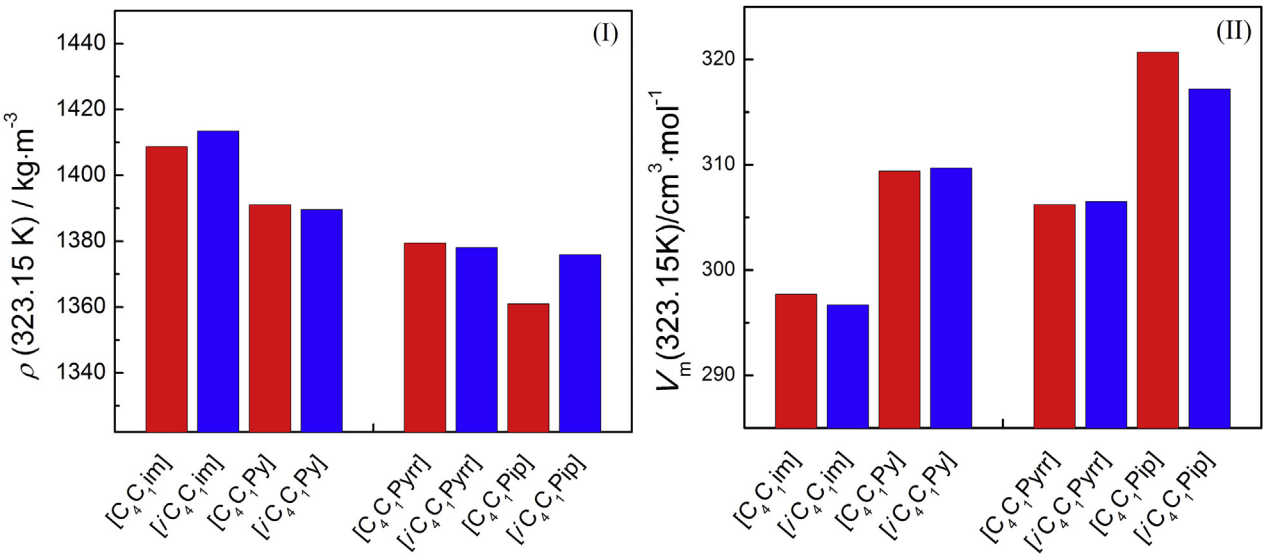

Fig. 4. Density (I) and molar volume (II), at 323.15 K and $p^{\circ} = 0.10 \pm 0.01$ MPa, as a function of the cations in the $[NTf_2]^-$-based ionic liquids. Literature: - $[C_4C_1im][NTf_2]$ [56].

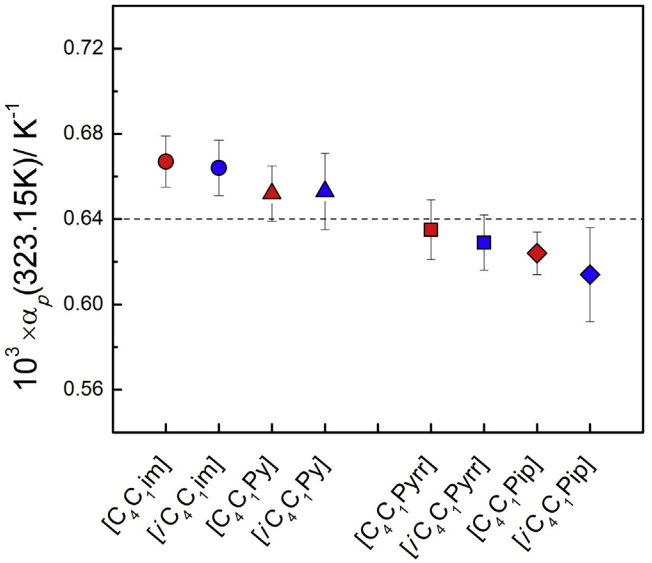

Fig. 5. Thermal expansion coefficients, α_p, at 323.15 K and $p^{\circ} = 0.10 \pm 0.01$ MPa, as a function of the cations in the $[NTf_2]$ based ionic liquids. Literature: (red) ● - $[C_4C_1im][NTf_2]$ [56]. This work: (blue) ● -$[iC_4C_1im][NTf_2]$; (red) ▲ - $[C_4C_1py][NTf_2]$; (blue) ▲ - $[iC_4C_1py][NTf_2]$; (red) ■ - $[C_4C_1pyrr][NTf_2]$; (blue) ■ - $[iC_4C_1pyrr][NTf_2]$; (red) ◆ - $[C_4C_1pip][NTf_2]$; (blue) ◆ - $[iC_4C_1pip][NTf_2]$. Uncertainties of the experimental results were assigned on the basis on the extended standard deviation of the experimental results ± 0.02 K^{-1}. The dash-dot is a guide line with no physical meaning. (For interpretation of the references to colour in this figure legend, the reader is referred to the web version of this article.)

with a 5 and 6 atoms ring cation cores in the *n* alkyl series with the former presenting higher surface entropy. This indicates a more efficient arrangement of the non-polar region at the surface for the smaller cation cores.

3.5. Refractive indices

The graphic representation of the refractive indices, as a function of the temperature for the studied ILs, is depicted in Fig. 8(I). The experimental data is presented in Table 8. The refractive indices of all studied ILs, at $T = 298.15$ K, along with available literature values, and the derivative of the temperature dependence of the refractive index, $\partial n_D/\partial T$ are presented in Table 9.

The plots of the refractive indices, at $T = 298.15$ K, as a function of the total number of carbon atoms in the alkyl chains in the imidazolium cations, for the measured ILs, are shown in Fig. 8 (II). The refractive indices obtained in this work are in good agreement with the available literature data, with relative deviations below 2%. Seki *et al.* [62] reported an experimental study of 17 ILs with different cations and anions, in the temperature range of 283.15–353.15 K. The authors [62] found that the refractive indices of pyridinium-based ILs are quite different from those of imidazolium and pyrrolidinium ILs. The refractive indices are barely dependent on the cation structure but are highly dependent on the anion. Our experimental results are consistent with the relations observed by Seki *et al.* [62] The higher refractive indices of the pyridinium-based ILs is related with the higher polarizability of the aromatic moieties in this aromatic ring.

Table 6
Experimental results of surface tension, γ (mN.m^{-1}), at $p^{\circ} = 0.10 \pm 0.01$ MPa, for the investigated ILs as a function of temperature.

T/K	γ (mN·m^{-1})				
	$[NTf_2]^-$				
	$[iC_4C_1im]^+$	$[iC_4C_1py]^+$	$[iC_4C_1pyrr]^+$	$[C_4C_1pip]^+$	$[iC_4C_1pip]^+$
298.2	32.72	33.45	33.54	34.14	
308.2	32.26	32.99	33.10	33.65	33.90
318.2	31.81	32.54	32.65	33.17	33.45
328.2	31.35	32.08	32.20	32.68	33.01
338.2	30.90	31.63	31.75	32.20	32.56
343.2	30.67	31.40	31.53	31.96	32.34

The expanded uncertainty, within 0.95 confidence level, for the surface tension and temperature data are ± 0.3 mN·m^{-1} and ±0.1 K respectively. The expanded uncertainty includes the calibration uncertainty. The results presented here were fitted with a linear equation from the raw data.

3.6. Viscosities

The experimental viscosities for the ILs here studied are reported in Table 10 and represented in Fig. 9. The experimental data was correlated using the Vogel-Tammann-Fulcher (VTF) model described in equation (9).

Table 7
Values of the surface tension γ (mN·m^{-1}) at 330.0 K and $p^{\circ} = 0.10 \pm 0.01$ MPa, and surface thermodynamic functions, S^{γ} (J K^{-1} m^{-2}) and H^{γ} (J m^{-2}).

Ionic liquid anion $[NTf_2]^-$	$\gamma \pm \sigma$ (330 K)/(mN·m^{-1})	$(S^{\gamma} \pm \sigma) \times 10^5$/(J·K^{-1}·m^{-2})	$(H^{\gamma} \pm \sigma)\times 10^2$/(J·m^{-2})
$[C_4C_1im]^+$ [60]	31.6 ± 0.5	5.5 ± 0.1	4.97 ± 0.03
$[iC_4C_1im]^+$	31.3 ± 0.8	4.5 ± 0.1	4.63 ± 0.06
$[C_4C_1py]^+$	32.0 ± 0.2	4.9 ± 0.1	4.82 ± 0.01
$[iC_4C_1py]^+$	32.0 ± 0.6	4.6 ± 0.1	4.70 ± 0.05
$[C_4C_1pyrr]^+$ [61]	32.7 ± 0.6	5.9 ± 0.1	5.21 ± 0.04
$[iC_4C_1pyrr]^+$	32.1 ± 0.4	4.5 ± 0.1	4.69 ± 0.03
$[C_4C_1pip]^+$	32.6 ± 0.4	4.9 ± 0.1	4.86 ± 0.03
$[iC_4C_1pip]^+$	32.9 ± 0.5	4.5 ± 0.1	4.77 ± 0.03

σ – overall uncertainty for 0.95 level of confidence.

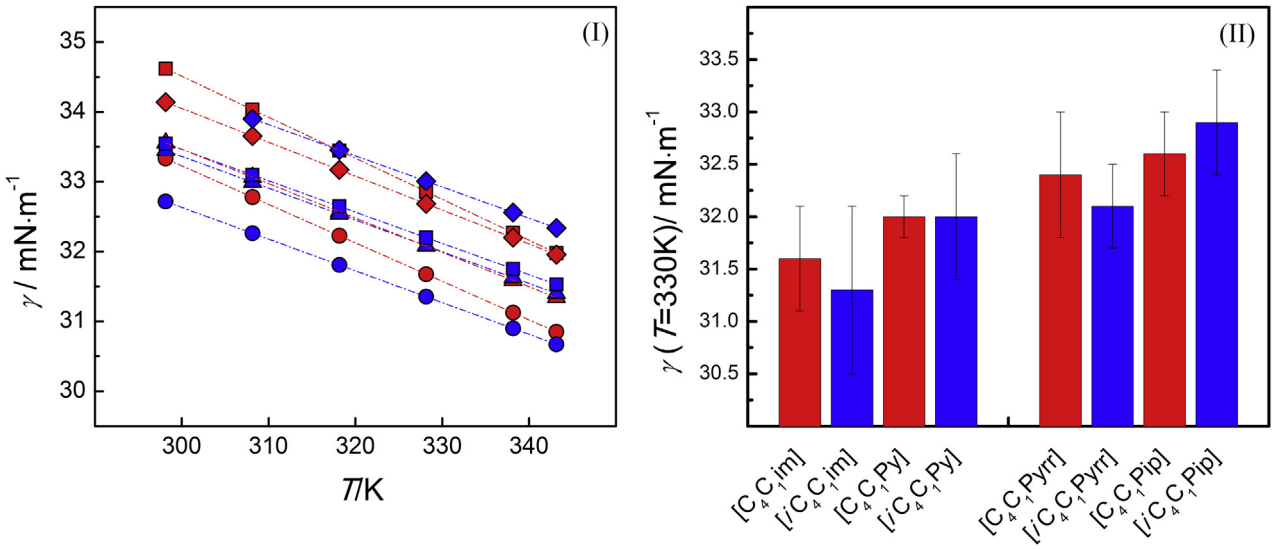

Fig. 6. Surface tension values of ILs as function of temperature (I). Literature: (red) ● - $[C_4C_1im][NTf_2]$; (red) [60]; ■ - $[C_4C_1pyrr][NTf_2]$ [61]. This work: (blue) ● - $[iC_4C_1im][NTf_2]$; (red) ▲ - $[C_4C_1py][NTf_2]$; (blue) ▲ - $[iC_4C_1py][NTf_2]$; (blue) ■ - $[iC_4C_1pyrr][NTf_2]$; (red) ◆ - $[C_4C_1pip][NTf_2]$; (blue) ◆ -$[iC_4C_1pip][NTf_2]$. Surface tension dependence, at 330 K, as a function of the cations in the $[NTf_2]$-based ionic liquids (II). (For interpretation of the references to colour in this figure legend, the reader is referred to the web version of this article.)

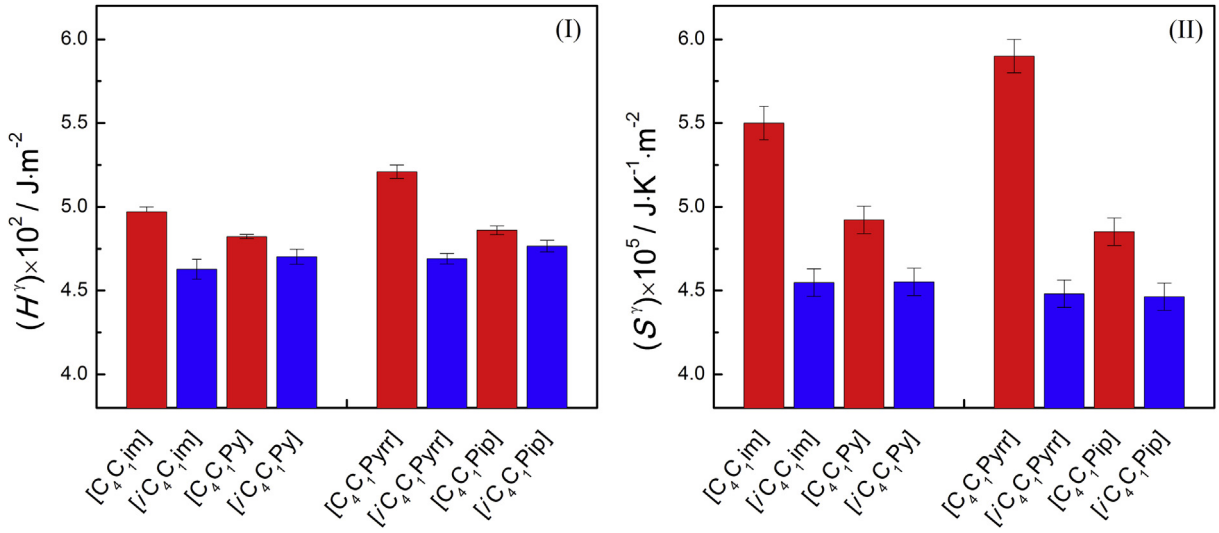

Fig. 7. Surface enthalpies and entropies as a function of the cations in the $[NTf_2]$-based ionic liquids. Enthalpy (**I**); Entropy (**II**). Literature: - $[C_4C_1im][NTf_2]$ [60]; $[C_4C_1pyrr][NTf_2]$ [61].

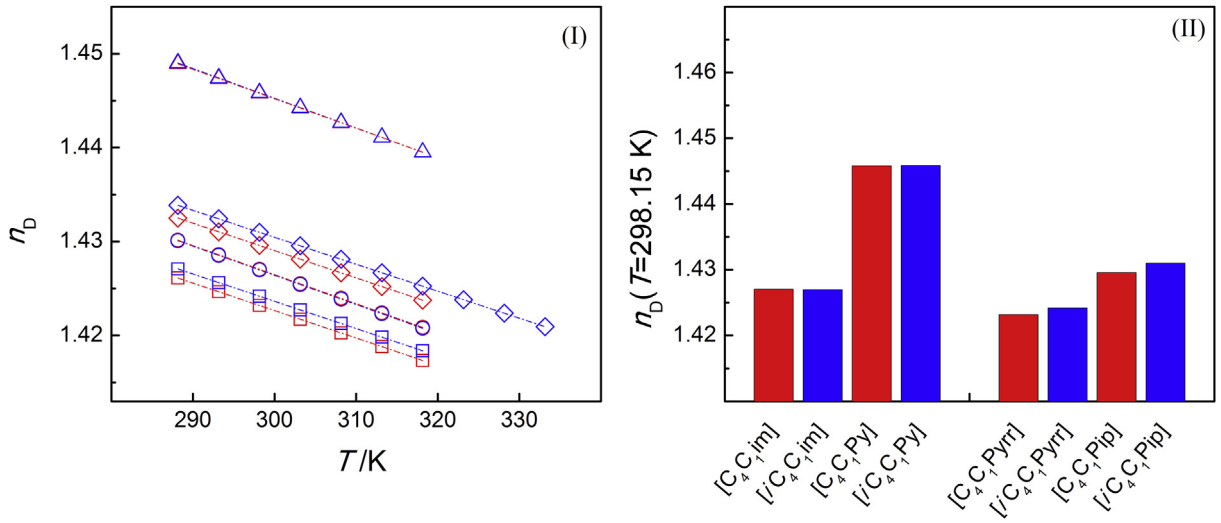

Fig. 8. Refractive indices as a function of temperature at $p^{o} = 0.10 \pm 0.01$ MPa for the studied ILs **(I)**. (red) ○ -[C_4C_1im][NTf_2]; (blue) ○-[iC_4C_1im][NTf_2]; (red) △ - [C_4C_1py][NTf_2]; (blue) △ - [iC_4C_1py][NTf_2]; (red) □ - [C_4C_1pyrr][NTf_2]; (blue) □ - [iC_4C_1pyrr][NTf_2]; (red) ◇ - [C_4C_1pip][NTf_2]; (blue) ◇ - [iC_4C_1pip][NTf_2]. Refractive indices, n_D, at $T = 298.15$ K as a function of as a function of the cations in the $[NTf_2]^-$-based ionic liquids **(II)**. (For interpretation of the references to colour in this figure legend, the reader is referred to the web version of this article.)

Table 8
Experimental refractive indices at the sodium D-line, n_D, for the studied ILs as a function of temperature T at $p^{\circ} = 0.10 \pm 0.01$ MPa.

T/K	n_D			
	$[C_4C_1im]^+$	$[iC_4C_1im]^+$	$[C_4C_1py]$	$[iC_4C_1py]^+$
288.15	1.4302	1.4301	1.4490	1.4490
293.15	1.4286	1.4285	1.4474	1.4474
298.15	1.4270	1.4270	1.4460	1.4459
303.15	1.4255	1.4254	1.4442	1.4443
308.15	1.4240	1.4239	1.4427	1.4427
313.15	1.4224	1.4223	1.4411	1.4411
318.15	1.4209	1.4208	1.4395	1.4395
	$[C_4C_1pyrr]^+$	$[iC_4C_1pyrr]^+$	$[C_4C_1pip]^+$	$[iC_4C_1pip]^+$
288.15	1.4261	1.4271	1.4325	1.4339
293.15	1.4247	1.4256	1.4311	1.4324
298.15	1.4232	1.4242	1.4296	1.4310
303.15	1.4217	1.4227	1.4281	1.4300
308.15	1.4203	1.4213	1.4267	1.4281
313.15	1.4188	1.4198	1.4252	1.4267
318.15	1.4173	1.4184	1.4238	1.4252
323.15				1.4238
328.15				1.4224
333.15				1.4209

The expanded uncertainty, within 0.95 confidence level, for the surface tension and temperature data are ± 0.00005 and ± 0.1 K respectively. The expanded uncertainty includes the calibration uncertainty. The results presented here were fitted with a linear equation from the raw data.

$$\ln(\eta/\text{mPa}\cdot\text{s}) = \ln(A_\eta/\text{mPa}\cdot\text{s}) + \frac{B_\eta}{(T - C_\eta)} \quad (9)$$

where η is the viscosity in mPa·s, T is the temperature in K, and A_η, B_η and C_η are the fitting coefficients derived from experimental data.

The energy barrier of the fluid to shear was evaluated based on the viscosity dependence with the temperature using equation (10):

$$E = R\cdot\frac{\partial(\ln\eta)}{\partial(1/T)} = R\cdot\left(\frac{B_\eta}{\left(\frac{C_\eta^2}{T^2} - \frac{2\cdot C_\eta}{T} + 1\right)}\right) \quad (10)$$

where A_η, B_η and C_η are the coefficients derived from the VTF equation (9), and the viscosity and the derived energy barrier, E, at $T = 323.15$ K, are presented in Table 11.

The viscosities of the studied compounds, η, at $T = 323.15$ K, are depicted in Fig. 10. The pre-exponential coefficient of the VTF equation, A_η, and the energy barrier at $T = 323.15$ K, E ($T = 323.15$ K), as a function of the cation are represented in Fig. 11.

Fig. 10 shows a clear differentiation between the aromatic and non-aromatic ILs. In aromatic ILs, the *iso*-alkyl IL presents a higher viscosity than the *n*-alkyl while the opposite was observed for the non-aromatic ILs. A detailed analysis of the shear stress energetics of the viscosity, depicted in Fig. 11, shows that the *iso*-alkyl aromatic ILs present a higher energy barrier, in line with the observed in the viscosity trend. For the non-aromatic ILs, the *iso*-alkyl group leads to a decrease in the energy barrier that is driving the

Table 9
Experimental refractive indices at the sodium D-line, n_D, for the studied ILs at $T = 298.15$ and $p^{\circ} = 0.10 \pm 0.01$ MPa and respective available literature data. Derivative of the temperature dependence of the refractive index, $\partial n_D/\partial T$.

Ionic liquid	n_D (298.15 K)	$10^4\cdot(\partial n_D/\partial T)/(K^{-1})$ [j]	n_D (298.15 K) literature
$[C_4C_1im][NTf_2]$	1.4271	−3.10 ± 0.01	n.a.
$[iC_4C_1im][NTf_2]$	1.4270	−3.09 ± 0.01	n.a.
$[C_4C_1py][NTf_2]$	1.4460	−3.14 ± 0.01	1.44566 ± 0.00037[k] 1.44594 ± 0.00048[l] 1.4460 ± 0.0007[m]
$[iC_4C_1py][NTf_2]$	1.4460	−3.17 ± 0.01	n.a.
$[C_4C_1pyrr][NTf_2]$	1.4232	−2.93 ± 0.01	1.42304 ± 0.00037[n] 1.42302 ± 0.00046 1.4202 ± 0.0033[o]
$[iC_4C_1pyrr][NTf_2]$	1.4242	−2.91 ± 0.01	n.a.
$[C_4C_1pip][NTf_2]$	1.4300	−2.92 ± 0.01	1.42928 ± 0.00037[k]
$[iC_4C_1pip][NTf_2]$	1.4310[p]	−2.87 ± 0.01	n.a.

[j] in the temperature interval, any value of n_D, at a specific temperature, T, can be estimated using the following equation: $n_D(T/K) = n_D$ (298.15 K) + $dn_D/dT\cdot(T/K$ - 298.15 K). n.a. stands for non-available data. Literature data: [k] [24]; [l] [63]; [m] [64]; [n] [65]; [o] [66]. [p] extrapolated value to 298.15 K from the linear fitting of $n_D = f(T)$. The data presented in this table was obtained taking into account the linear fitting of the raw experimental results for the refractive indices. Uncertainty associated to n_D (298.15 K) of ± 0.0002, is the extended standard deviation and was estimated from the combined uncertainty of the calibration and the two set of independent refractive indices measurements.

Table 10
Experimental viscosity results, η, at $p^{\circ} = 0.10 \pm 0.01$ MPa for the studied ILs as a function of temperature.

T/K	η/(mPa·s)						
	$[iC_4C_1im]^+$	$[C_4C_1py]^+$	$[iC_4C_1py]^+$	$[C_4C_1pip]^+$	$[iC_4C_1pip]^+$	$[C_4C_1pyrr]^+$	$[iC_4C_1pyrr]^+$
	$[NTf_2]^-$						
293.15	107.35	84.20	135.42	261.28		101.71	83.61
298.15	81.44	65.74	100.10	189.11		79.57	66.29
303.15	63.36	52.39	76.34	141.44	125.12	63.64	53.53
308.15	50.30	42.46	59.56	108.27	96.40	51.71	43.91
313.15	40.69	34.93	47.48	84.87	76.03	42.67	36.52
318.15	33.40	29.13	38.42	67.24	60.67	35.60	30.75
323.15	27.81	24.59	31.63	54.34	49.34	30.07	26.18
328.15	23.46	20.97	26.40	44.55	40.71	25.66	22.52
333.15	20.05	18.10	22.36	37.09	34.11	22.16	19.57
338.15	17.24	15.71	19.08	31.09	28.76	19.21	17.09
343.15	14.99	13.77	16.47	26.41	24.57	16.83	15.06
348.15	13.14	12.15	14.35	22.65	21.18	14.84	13.36
353.15	11.63	10.82	12.63	19.65	18.47	13.21	11.95
358.15	10.31	9.66	11.14	17.09	16.14	11.77	10.70
363.15	9.22	8.69	9.93	15.01	14.25	10.57	9.65

The magnitude of the experimental differentiation between the two independent set of viscosity data: ± [0.005 mPa s + 0.001.(η/mPa s)].

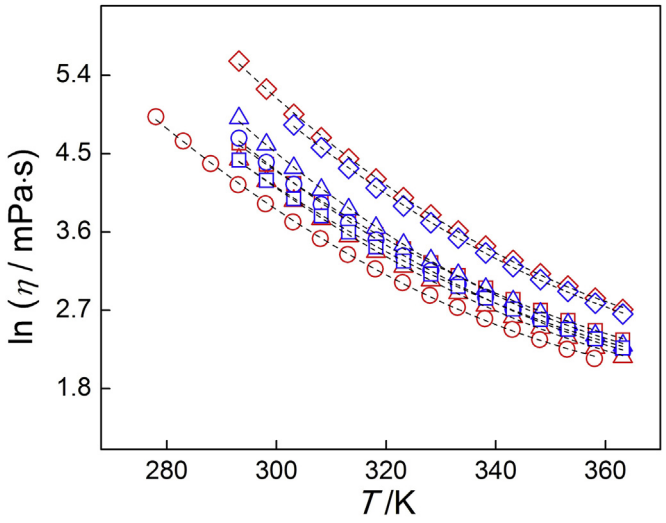

Fig. 9. Logarithm of viscosity as a function of temperature at $p^{\circ} = 0.10 \pm 0.01$ MPa for the studied ILs. The solid lines represent the Vogel-Tammann-Fulcher fitting from equation (9). (blue) ○ - $[iC_4C_1im][NTf_2]$; (red) △ - $[C_4C_1py][NTf_2]$; (blue) △ - $[iC_4C_1py][NTf_2]$; (red) □ - $[C_4C_1pyrr][NTf_2]$; (blue) □ - $[iC_4C_1pyrr][NTf_2]$; (red) ◇ - $[C_4C_1pip][NTf_2]$; (blue) ◇ - $[iC_4C_1pip][NTf_2]$. (For interpretation of the references to colour in this figure legend, the reader is referred to the web version of this article.)

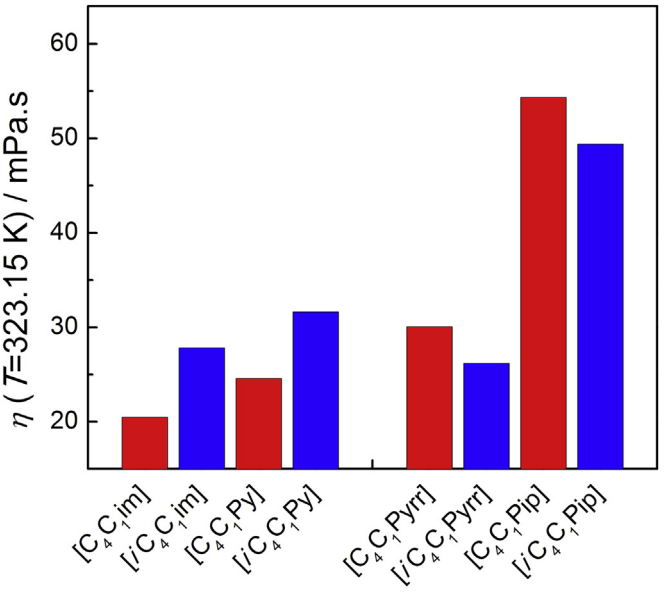

Fig. 10. Viscosity (η/mPa s) at $T = 323.15$ K and $p^{\circ} = 0.10 \pm 0.01$ MPa as a function of the cations in the $[NTf_2]$-based ionic liquids. Literature: (red) ● -$[C_4C_1im][NTf_2]$ [56]. This work: (blue) ● - $[iC_4C_1im][NTf_2]$; (red) ▲ - $[C_4C_1py][NTf_2]$; (blue) ▲ - $[iC_4C_1py][NTf_2]$; (red) ■ - $[C_4C_1pyrr][NTf_2]$; (blue) ■ - $[iC_4C_1pyrr][NTf_2]$; (red) ◆ - $[C_4C_1pip][NTf_2]$; (blue) ◆ - $[iC_4C_1pip][NTf_2]$. (For interpretation of the references to colour in this figure legend, the reader is referred to the web version of this article.)

decrease in the viscosity, when compared with the respective *n*-alkyl isomers. As expected, the branching of the alkyl side chain increases the pre-exponential coefficient, A_η for all compounds studied. The piperidinium-based ILs are the most viscous as a result of the higher energy barrier, which must be related to conformational features. The larger number of possible

Table 11
Fitted parameters of VTF equation for the viscosity data of the studied ILs, viscosity and the derived energy barrier at $T = 323.15$ K and $p^{\circ} = 0.10 \pm 0.01$ MPa.

Ionic liquid	A_η/(mPa.s)	B_η/K	C_η/K	η/(mPa·s)	E/(kJ·mol^{-1})
				($T = 323.15$ K)	
$[iC_4C_1im][NTf_2]$	0.1909 ± 0.004	701.9 ± 6.0	182.3 ± 0.6	27.82	30.70 ± 0.64
$[C_4C_1py][NTf_2]$	0.1725 ± 0.002	748.8 ± 4.2	172.2 ± 0.4	24.59	28.52 ± 0.37
$[iC_4C_1py][NTf_2]$	0.2058 ± 0.004	675.3 ± 5.6	189.0 ± 0.5	31.64	32.60 ± 0.69
$[C_4C_1pip][NTf_2]$	0.1571 ± 0.004	830.1 ± 7.8	181.2 ± 0.7	54.36	35.76 ± 0.82
$[iC_4C_1pip][NTf_2]$	0.1793 ± 0.005	791.8 ± 8.4	182.2 ± 0.8	49.40	34.61 ± 0.94
$[C_4C_1pyrr][NTf_2]$	0.1779 ± 0.005	803.3 ± 8.0	166.6 ± 0.8	30.07	28.44 ± 0.65
$[iC_4C_1pyrr][NTf_2]$	0.1949 ± 0.005	768.8 ± 7.7	166.3 ± 0.8	26.19	27.12 ± 0.62

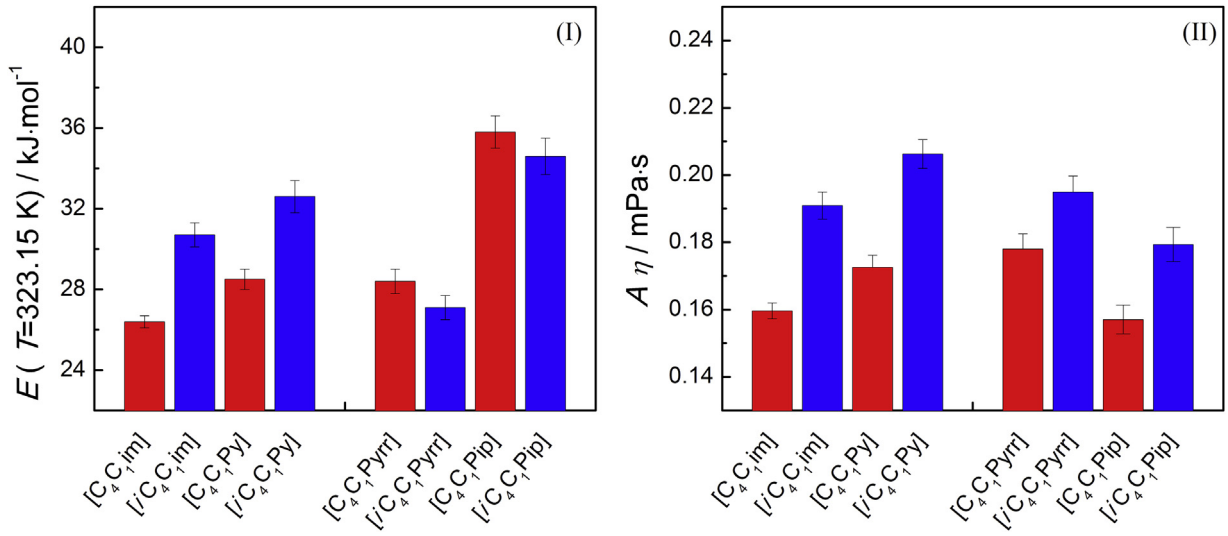

Fig. 11. The energy barrier (E/kJ mol^{-1}) at 323.15 K **(I)** and Pre-exponential coefficient of the VTF equation (A_η/mPa s) **(II)** as a function of the cations in the [NTf_2]-based ionic liquids.

conformations increases the cohesive interaction in the shear, thus increasing the viscosities.

3.7. Final remarks

The *n* vs. *iso* isomerization, aromaticity and ring cation core size effects on the physical-chemical properties of ionic liquids (ILs), such as thermal behaviour, heat capacities, densities, refractive indices, surface tensions and kinematic viscosities were explored in this work. From the temperature dependence of the experimental results, the thermal expansion coefficients, the thermal temperature dependence of the refractive index, entropies and enthalpies of surface formation and energy barrier to shear were derived. This study highlights that the incorporation of a branched alkyl chain in different types and sizes of aromatic and non-aromatic cations cannot be easily interpreted and generalized.

We found that the *iso*-alkyl group leads to an increase in the relative stability of the glass relative to the supercooled liquid, leading to higher T_g. The heat capacity change of the glass transition enhances the absolute entropic differentiation between the glass and liquid states. The *iso*-pyrrolidinium (5 atoms ring cation core) and *iso*-piperidinium (6 atoms ring cation core) ILs present a strong differentiation in the enthalpy and entropy of melting.

Non-aromatic ILs present a higher molar heat capacity due to the increase of the atomic contribution. No significant differentiation on the isomerization *n* to *iso*-alkyl ILs was found in the heat capacities. The *n* to *iso* isomerization has no effect on the densities and thermal expansion; nevertheless, these properties are sensitive to the aromaticity of the cation core.

No *n* to *iso* differentiation and a very small increase (from the 5 to 6 ring cation core) in refractive indices was observed. The pyridinium cations derived ILs were those with the highest refractive indices which are related with the higher polarizability of the aromatic pyridinium ring. The temperature dependence of the refractive indices is in the range between $-(2.9–3.2) \times 10^{-4}$ K^{-1} and seems to be related with the thermal expansion coefficients of each ILs.

The small increase of the surface tension from the aromatic to the non-aromatic ILs was found to be related with the higher cohesive energy of the bulk in non-aromatic ILs and the slightly lower surface entropy of the *iso* isomers, an indication of a strong structural resemblance between the bulk and the IL surface. The significant differentiation between IL with 5 and 6 atoms ring cation cores in the *n*-alkyl series (5 atoms ring cation has higher surface entropy) is an indication of a more efficient arrangement of the non-polar region at the surface in the smaller cation core.

The non-aromatic piperidinium cation and the *iso*-alkyl isomers were found to be the most viscous among the studied ILs, due to their higher energy barrier which can also be related with conformational features. A larger number of possible conformations will increase the cohesive interaction on the shear.

Acknowledgments

Thanks are due to Fundação para a Ciência e Tecnologia (FCT), Lisbon, Portugal and to FEDER for financial support to Centro de Investigação em Química, University of Porto through the project Pest-C/QUI/UI0081/2013, and CICECO, University of Aveiro, through the project Pest-C/CTM/LA0011/2013,financed by national funds through the FCT/MEC and when applicable co-financed by FEDER under the PT2020 Partnership Agreement, and COST action CM1206- EXIL - Exchange on Ionic Liquids. The authors also thank FCT for the PhD grants SFRH/BD/81261/2011 from A.S.M.C. Rodrigues and SFRH/BD/88369/2012 from Hugo F. D. Almeida. M.G. Freire acknowledges the European Research Council (ERC) for the Starting Grant ERC-2013-StG-337753.

Appendix A. Supplementary data

Supplementary data related to this article can be found at http://dx.doi.org/10.1016/j.fluid.2016.04.009.

References

[1] M. Freemantle, An Introduction to Ionic Liquids, RSC Publishing, The Royal Society of Chemistry, 2009, http://dx.doi.org/10.1039/9781849737050.
[2] Y. Wang, G.A. Voth, Unique spatial heterogeneity in ionic liquids, J. Am. Chem. Soc. 127 (2005) 12192–12193, http://dx.doi.org/10.1021/ja053796g.
[3] S. Aparicio, M. Atilhan, F. Karadas, Thermophysical properties of pure ionic liquids: review of present situation, Ind. Eng. Chem. Res. 49 (2010) 9580–9595, http://dx.doi.org/10.1021/ie101441s.
[4] C.P. Fredlake, J.M. Crosthwaite, D.G. Hert, S.N.V.K. Aki, J.F. Brennecke, Thermophysical properties of imidazolium-based ionic liquids, J. Chem. Eng. Data 49 (2004) 954–964, http://dx.doi.org/10.1021/je034261a.
[5] T. Welton, Ionic liquids in catalysis, Coord. Chem. Rev. 248 (2004) 2459–2477, http://dx.doi.org/10.1016/j.ccr.2004.04.015.
[6] K.N. Marsh, A. Deev, A.C.-T. Wu, E. Tran, A. Klamt, Room temperature ionic

liquids as replacements for conventional solvents – a review, Korean J. Chem. Eng. 19 (2002) 357–362, http://dx.doi.org/10.1007/BF02697140.
[7] K.R. Seddon, Ionic liquids for clean technology, J. Chem. Technol. Biotechnol. 68 (1997) 351–356, http://dx.doi.org/10.1002/(SICI)1097-4660(199704)68:4<351::AID-JCTB613>3.0.CO;2–4.
[8] D. Rooney, J. Jacquemin, R. Gardas, Thermophysical properties of ionic liquids., in: Top. Curr. Chem., Springer, Berlin/Heidelberg, 2010, pp. 185–212, http://dx.doi.org/10.1007/128_2008_32.
[9] J.A.P. Coutinho, P.J. Carvalho, N.M.C. Oliveira, Predictive methods for the estimation of thermophysical properties of ionic liquids, RSC Adv. 2 (2012) 7322, http://dx.doi.org/10.1039/c2ra20141k.
[10] N. V Plechkova, K.R. Seddon, Applications of ionic liquids in the chemical industry, Chem. Soc. Rev. 37 (2008) 123–150, http://dx.doi.org/10.1039/b006677j.
[11] A.J. Carmichael, K.R. Seddon, Polarity study of some 1-alkyl-3-methylimidazolium ambient-temperature ionic liquids with the solvatochromic dye, Nile Red, J. Phys. Org. Chem. 13 (2000) 591–595, http://dx.doi.org/10.1002/1099-1395(200010)13:10<591::AID-POC305>3.0.CO;2–2.
[12] K. Paduszyński, U. Domańska, A new group contribution method for prediction of density of pure ionic liquids over a wide range of temperature and pressure, Ind. Eng. Chem. Res. 51 (2012) 591–604, http://dx.doi.org/10.1021/ie202134z.
[13] L.F. Vega, O. Vilaseca, F. Llovell, J.S. Andreu, Modeling ionic liquids and the solubility of gases in them: recent advances and perspectives, Fluid Phase Equilib. 294 (2010) 15–30, http://dx.doi.org/10.1016/j.fluid.2010.02.006.
[14] E.J. Maginn, J.R. Elliott, Historical perspective and current outlook for molecular dynamics as a chemical engineering tool, Ind. Eng. Chem. Res. 49 (2010) 3059–3078, http://dx.doi.org/10.1021/ie901898k.
[15] N. Rai, E.J. Maginn, Vapor–liquid coexistence and critical behavior of ionic liquids via molecular simulations, J. Phys. Chem. Lett. 2 (2011) 1439–1443, http://dx.doi.org/10.1021/jz200526z.
[16] M. Smiglak, A. Metlen, R.D. Rogers, The second evolution of ionic liquids: from solvents and separations to advanced materials–energetic examples from the ionic liquid cookbook, Acc. Chem. Res. 40 (2007) 1182–1192, http://dx.doi.org/10.1021/ar7001304.
[17] I. Bandrés, B. Giner, H. Artigas, F.M. Royo, C. Lafuente, Thermophysic comparative study of two isomeric pyridinium-based ionic liquids, J. Phys. Chem. B 112 (2008) 3077–3084.
[18] R.L. Gardas, H.F. Costa, M.G. Freire, P.J. Carvalho, I.M. Marrucho, I.M.A. Fonseca, et al., Densities and derived thermodynamic properties of imidazolium-, pyridinium-, pyrrolidinium-, and piperidinium-based ionic liquids, J. Chem. Eng. Data 53 (2008) 805–811, http://dx.doi.org/10.1021/je700670k.
[19] F.S. Oliveira, M.G. Freire, P.J. Carvalho, J.A.P. Coutinho, J.N.C. Lopes, L.P.N. Rebelo, et al., Structural and positional isomerism influence in the physical properties of pyridinium NTf2-based ionic liquids: pure and water-saturated mixtures, J. Chem. Eng. Data 55 (2010) 4514–4520.
[20] T. Mandai, H. Masu, M. Imanari, K. Nishikawa, Comparison between cycloalkyl- and n -alkyl-substituted imidazolium-based ionic liquids in physicochemical properties and reorientational dynamics, J. Phys. Chem. B 116 (2012) 2059–2064, http://dx.doi.org/10.1021/jp210273q.
[21] M. Vranes, S. Dozic, V. Djeric, S. Gadzuric, Physicochemical characterization of 1-butyl-3-methylimidazolium and 1-butyl-1-methylpyrrolidinium bis(trifluoromethylsulfonyl)imide, J. Chem. Eng. Data 57 (2012) 1072–1077, http://dx.doi.org/10.1021/je2010837.
[22] H.K. Kashyap, C.S. Santos, N.S. Murthy, J.J. Hettige, K. Kerr, S. Ramati, et al., Structure of 1-alkyl-1-methylpyrrolidinium bis(trifluoromethylsulfonyl) amide ionic liquids with linear, branched, and cyclic alkyl groups. J. Phys. Chem. B 117 (2013) 15328–15337, http://dx.doi.org/10.1021/jp403518j.
[23] A. Andresova, J. Storch, M. Traïkia, Z. Wagner, M. Bendova, P. Husson, Branched and cyclic alkyl groups in imidazolium-based ionic liquids: molecular organization and physico-chemical properties, Fluid Phase Equilib. 371 (2014) 41–49, http://dx.doi.org/10.1016/j.fluid.2014.03.004.
[24] A. Bhattacharjee, P.J. Carvalho, J.A.P. Coutinho, The effect of the cation aromaticity upon the thermophysical properties of piperidinium- and pyridinium-based ionic liquids,, Fluid Phase Equilib. 375 (2014) 80–88, http://dx.doi.org/10.1016/j.fluid.2014.04.029.
[25] P. Verdía, M. Hernaiz, E.J. González, E.A. Macedo, J. Salgado, E. Tojo, Effect of the number, position and length of alkyl chains on the physical properties of polysubstituted pyridinium ionic liquids, J. Chem. Thermodyn. 69 (2014) 19–26, http://dx.doi.org/10.1016/j.jct.2013.09.028.
[26] R. Tao, G. Tamas, L. Xue, S.L. Simon, E.L. Quitevis, Thermophysical properties of imidazolium-based ionic liquids: the effect of aliphatic versus aromatic functionality, J. Chem. Eng. Data 59 (2014) 2717–2724, http://dx.doi.org/10.1021/je500185r.
[27] L. Pison, K. Shimizu, G. Tamas, J.N.C. Lopes, E.L. Quitevis, M.F.C. Gomes, Solubility of n-butane and 2-methylpropane (isobutane) in 1-alkyl-3-methylimidazolium-based ionic liquids with linear and branched alkyl side-chains, Phys. Chem. Chem. Phys. 17 (2015) 30328–30342, http://dx.doi.org/10.1039/c5cp05572e.
[28] Y. Zhang, L. Xue, F. Khabaz, R. Doerfler, E.L. Quitevis, R. Khare, et al., Molecular topology and local dynamics govern the viscosity of imidazolium-based ionic liquids, J. Phys. Chem. B 119 (2015) 14934–14944, http://dx.doi.org/10.1021/acs.jpcb.5b08245.
[29] T. Erdmenger, J. Vitz, F. Wiesbrock, U.S. Schubert, Influence of different branched alkyl side chains on the properties of imidazolium-based ionic liquids, J. Mater. Chem. 18 (2008) 5267, http://dx.doi.org/10.1039/b807119e.
[30] P.J. Carvalho, S.P.M. Ventura, M.L.S. Batista, B. Schröder, F. Gonçalves, J. Esperança, et al., Understanding the impact of the central atom on the ionic liquid behavior: phosphonium vs ammonium cations, J. Chem. Phys. 140 (2014) 064505, http://dx.doi.org/10.1063/1.4864182.
[31] E.L. Xue, L. Tamas, G. Koh, Y. P. Shadeck, M. Gurung, E. Simon, S. L. Maroncelli, M. Quitevis, Effect of alkyl branching on physicochemical properties of imidazolium-based ionic liquids, J. Chem. Eng. Data. (n.d.). doi:10.1021/acs.jced.5b00658.
[32] M.E. Wieser, M. Berglund, Atomic weights of the elements 2007 (IUPAC technical report), Pure Appl. Chem. 81 (2009) 2131–2156.
[33] C. Sabbah, A. Xu-wu, J.S. Chickos, M.L.P. Leitão, M.V. Roux, L.A. Torres, et al., Reference materials for calorimetry and differential thermal analysis, Thermochim. Acta 331 (1999) 93–204, http://dx.doi.org/10.1016/S0040-6031(99)00009-X.
[34] M.V. Roux, M. Temprado, J.S. Chickos, Y. Nagano, Critically evaluated thermochemical properties of polycyclic aromatic hydrocarbons, J. Phys. Chem. Ref. Data 37 (2008) 1855.
[35] A.V. Blokhin, Y.U. Paulechka, G.J. Kabo, Thermodynamic properties of [C 6 mim][NTf 2] in the condensed state, J. Chem. Eng. Data 51 (2006) 1377–1388, http://dx.doi.org/10.1021/je060094d.
[36] Y.U. Paulechka, A.V. Blokhin, G.J. Kabo, A.A. Strechan, Thermodynamic properties and polymorphism of 1-alkyl-3-methylimidazolium bis(triflamides), J. Chem. Thermodyn. 39 (2007) 866–877, http://dx.doi.org/10.1016/j.jct.2006.11.006.
[37] I.W.J. Konicek, J. Suurkuusk, A precise drop heat capacity calorimeter for small samples,, Chem. Scr. 1 (1971) 217–220.
[38] J. Suurkuusk, I. Wadsö, Design and testing of an improved precise drop calorimeter for the measurement of the heat capacity of small samples, J. Chem. Thermodyn. 6 (1974) 667–679, http://dx.doi.org/10.1016/0021-9614(74)90117-7.
[39] L.M.N.B.F. Santos, M.A.A.A. Rocha, A.S.M.C.M.C. Rodrigues, V. Štejfa, M. Fulem, M. Bastos, Reassembling and testing of a high-precision heat capacity drop calorimeter. Heat capacity of some polyphenyls at T=298.15K, J. Chem. Thermodyn. 43 (2011) 1818–1823, http://dx.doi.org/10.1016/j.jct.2011.06.010.
[40] International Association for the Properties of Water Steam, Viscosity of thermal conductivity of heavy water substance, physical chemistry of aqueous systems, in: Proc. 12th Int. Conf. Prop. Water Steam, Orlando, FL, 1994.
[41] G.R. Somayajulu, A generalized equation for surface tension from the triple point to the critical point, Int. J. Thermophys. 9 (1988) 559–566, http://dx.doi.org/10.1007/BF00503154.
[42] J.J. Jasper, E.V. Kring, The isobaric surface tensions and thermodynamic properties of the surfaces of a series of n-alkanes, C 5 to C 18, 1-alkenes, C 6 to C 16, and of n-decylcyclopentane, n-decylcyclohexane and n-dcylbenzene, J. Phys. Chem. 59 (1955) 1019–1021, http://dx.doi.org/10.1021/j150532a006.
[43] Z. Gu, J.F. Brennecke, Volume expansivities and isothermal compressibilities of imidazolium and pyridinium-based ionic liquids, J. Chem. Eng. Data 47 (2002) 339–345, http://dx.doi.org/10.1021/je010242u.
[44] R. Gomes de Azevedo, J.M.S.S. Esperança, J. Szydlowski, Z.P. Visak, P.F. Pires, H.J.R. Guedes, et al., Thermophysical and thermodynamic properties of ionic liquids over an extended pressure range: [bmim][NTf2] and [hmim][NTf2], J. Chem. Thermodyn. 37 (2005) 888–899, http://dx.doi.org/10.1016/j.jct.2005.04.018.
[45] R.L. Gardas, M.G. Freire, P.J. Carvalho, I.M. Marrucho, I.M.A. Fonseca, A.G.M. Ferreira, et al., High-pressure densities and derived thermodynamic properties of imidazolium-based ionic liquids, J. Chem. Eng. Data 52 (2007) 80–88, http://dx.doi.org/10.1021/je060247x.
[46] M.G. Freire, P.J. Carvalho, A.M. Fernandes, I.M. Marrucho, A.J. Queimada, J.A.P. Coutinho, Surface tensions of imidazolium based ionic liquids: anion, cation, temperature and water effect. J. Colloid Interface Sci. 314 (2007) 621–630, http://dx.doi.org/10.1016/j.jcis.2007.06.003.
[47] P.J. Carvalho, M.G. Freire, I.M. Marrucho, A.J. Queimada, J.A.P. Coutinho, Surface tensions for the 1-alkyl-3-methylimidazolium bis(trifluoromethylsulfonyl)imide ionic liquids, J. Chem. Eng. Data 53 (2008) 1346–1350, http://dx.doi.org/10.1021/je800069z.
[48] H. Tokuda, K. Hayamizu, K. Ishii, M.A.B.H. Susan, M. Watanabe, Physicochemical properties and structures of room temperature ionic liquids. 2. Variation of alkyl chain length in imidazolium cation, J. Phys. Chem. B 109 (2005) 6103–6110, http://dx.doi.org/10.1021/jp044626d.
[49] S. V Dzyuba, R.A. Bartsch, Influence of structural variations in 1-alkyl(aralkyl)-3-methylimidazolium hexafluorophosphates and bis(trifluoromethylsulfonyl)imides on physical properties of the ionic liquids, Chem. Phys. Chem. 3 (2002) 161–166, http://dx.doi.org/10.1002/1439-7641(20020215)3:2<161::AID-CPHC161>3.0.CO;2–3.
[50] A.S. Rodrigues, L.M.N.B.F. Santos, Nanostructuration effect on the thermal behaviourof ionic liquids, Chem. Phys. Chem. (2016), http://dx.doi.org/10.1002/cphc.201501128.
[51] Y.U. Paulechka, A.G. Kabo, A. V Blokhin, G.J. Kabo, M.P. Shevelyova, Heat capacity of ionic liquids: experimental determination and correlations with molar volume, J. Chem. Eng. Data 55 (2010) 2719–2724, http://dx.doi.org/10.1021/je900974u.
[52] J.G. Aston, G.H. Messerly, The heat capacity and entropy, heats of fusion and vaporization and the vapor pressure of n-butane 1, J. Am. Chem. Soc. 62

(1940) 1917–1923, http://dx.doi.org/10.1021/ja01865a005.
[53] J.G. Aston, R.M. Kennedy, S.C. Schumann, G.H. Messerly, The heat capacity and entropy, heats of fusion and vaporization and the vapor pressure of isobutane, J. Am. Chem. Soc. 62 (1940) 1917–1923, http://dx.doi.org/10.1021/ja01865a005.
[54] M.A.A. Rocha, M. Bastos, J.A.P. Coutinho, L.M.N.B.F. Santos, Heat capacities at 298.15 K of the extended [CnC1im][NTf_2] ionic liquid series, J. Chem. Thermodyn. 53 (2012) 140–143, http://dx.doi.org/10.1016/j.jct.2012.04.025.
[55] R.L. Gardas, J.A.P. Coutinho, A group contribution method for heat capacity estimation of ionic liquids, Ind. Eng. Chem. Res. 47 (2008) 5751–5757, http://dx.doi.org/10.1021/ie800330v.
[56] M.A.A. Rocha, C.M.S.S. Neves, M.G. Freire, O. Russina, A. Triolo, J.A.P. Coutinho, et al., Alkylimidazolium based ionic liquids: impact of cation symmetry on their nanoscale structural organization, J. Phys. Chem. B 117 (2013) 10889–10897, http://dx.doi.org/10.1021/jp406374a.
[57] A.W. Adamson, A.P. Gast, Physical Chemistry of Surfaces, John Wiley, New York, 1997.
[58] J.C. Miller, J.N. Miller, Statistical for Analytical Chemistry, Hall, PTR Prentice, Chichester, NY, 1993.
[59] H.F.D. Almeida, M.G. Freire, A.M. Fernandes, J.A. Lopes-da-Silva, L.M.N.B.F. Santos, J.A.P. Coutinho, et al., Cation alkyl side chain length and symmetry effects on the surface tension of ionic liquids, Langmuir 30 (2014) 6408–6418, http://dx.doi.org/10.1021/la501308q.
[60] P.J. Carvalho, M.G. Freire, I.M. Marrucho, A.J. Queimada, J.A.P. Coutinho, Surface tensions for the 1-alkyl-3-methylimidazolium bis(trifluoromethylsulfonyl) imide ionic liquids, J. Chem. Eng. Data 53 (2008) 1346–1350.
[61] P.J. Carvalho, C.M.S.S. Neves, J.A.P. Coutinho, Surface tensions of bis(trifluoromethylsulfonyl)imide anion-based ionic liquids, J. Chem. Eng. Data 55 (2010) 3807–3812, http://dx.doi.org/10.1021/je100253m.
[62] S. Seki, S. Tsuzuki, K. Hayamizu, Y. Umebayashi, N. Serizawa, K. Takei, et al., Comprehensive refractive index property for room-temperature ionic liquids, J. Chem. Eng. Data 57 (2012) 2211–2216.
[63] R.G. Seoane, S. Corderí, E. Gómez, N. Calvar, E.J. González, E.A. Macedo, et al., Temperature dependence and structural influence on the thermophysical properties of eleven commercial ionic liquids, Ind. Eng. Chem. Res. 51 (2012) 2492–2504, http://dx.doi.org/10.1021/ie2029255.
[64] S. Corderí, B. González, Ethanol extraction from its azeotropic mixture with hexane employing different ionic liquids as solvents, J. Chem. Thermodyn. 55 (2012) 138–143, http://dx.doi.org/10.1016/j.jct.2012.06.028.
[65] A.B. Pereiro, H.I.M. Veiga, J.M.S.S. Esperança, A. Rodríguez, Effect of temperature on the physical properties of two ionic liquids, J. Chem. Thermodyn. 41 (2009) 1419–1423, http://dx.doi.org/10.1016/j.jct.2009.06.020.
[66] M. Shamsipur, A.A.M. Beigi, M. Teymouri, S.M. Pourmortazavi, M. Irandoust, Physical and electrochemical properties of ionic liquids 1-ethyl-3-methylimidazolium tetrafluoroborate, 1-butyl-3-methylimidazolium trifluoromethanesulfonate and 1-butyl-1-methylpyrrolidinium bis(trifluoromethylsulfonyl)imide, J. Mol. Liq. 157 (2010) 43–50, http://dx.doi.org/10.1016/j.molliq.2010.08.005.